Extended x-ray—absorption fine-structure study of anharmonicity in CuBr

J. M. Tranquada and R. Ingalls

Department of Physics, University of Washington, Seattle, Washington 98195
(Received 15 February 1983)

The extended x-ray—absorption fine structure (EXAFS) above the Cu and Br K edges in CuBr has been measured at 72, 210, and 295 K. The first-shell contributions were isolated by Fourier filtering the EXAFS data, and the resulting single-shell data were analyzed using the ratio method. It is found that the third and fourth cumulants of the nearest-neighbor distance distribution are quite significant even at 210 K and cannot be ignored when making least-squares fits to amplitude ratios and phase differences. At 295 K we obtain values of $(0.37\pm0.05)\times10^{-3}$ Å^3 and $(0.72\pm0.12)\times10^{-4}$ Å^4 for the third and fourth cumulants, respectively, as well as an anharmonic contribution of $(0.16\pm0.12)\times10^{-2}$ Å^2 to the mean-square relative displacement. The data cannot be explained by a disorder model in which a Cu ion is allowed to occupy four equivalent off-center sites as well as its ideal position; the non-Gaussian contribution must be due to intrinsic anharmonicity. Interpretation of the results in terms of an anharmonic effective single-particle potential for the Cu ions indicates that the fourth-order potential term is just as important as the third and cannot be neglected. This model gives a reasonable description of the temperature dependence of the second, third, and fourth cumulants.

I. INTRODUCTION

Extended x-ray—absorption fine-structure (EXAFS) spectroscopy is a useful probe of short-range pair-distribution functions in solids.[1] From measurements of EXAFS at more than one temperature, one can determine changes in these distributions. In a harmonic crystal, the distribution function for pairs of atoms whose equilibrium sites are separated by a particular lattice vector is determined by the phonon spectrum. The lattice vibrations contribute a Debye-Waller—type term $\exp(-2\sigma_j^2 k^2)$ to the EXAFS interference function $\chi(k)$,[2-4] where k is the photoelectron wave number. The term σ_j^2 in the exponent is the second cumulant of the interatomic distance distribution and can be expressed to first order as

$$\sigma_j^2 = \langle [(\vec{u}_j - \vec{u}_0)\cdot\hat{R}_j]^2 \rangle , \qquad (1)$$

where $\vec{u}_j$ is the displacement of atom j from its equilibrium site, $\hat{R}_j$ is a unit vector at the origin pointing towards site j, and the brackets denote a thermal average. In a harmonic crystalline material, cumulants beyond the second are zero and the effects of thermal vibrations on the EXAFS amplitude are fully characterized by σ_j^2. When the quasiharmonic approximation applies, σ_j^2 still gives a complete description of the interatomic distance distribution, but it is determined by a slightly different phonon spectrum at each temperature. However, when phonon-phonon interactions are important, higher cumulants must be included in the EXAFS formula.[4] The even cumulants contribute to the amplitude of $\chi(k)$ while the odd cumulants enter the phase, and the nth cumulant appears multiplied by the nth power of the photoelectron wave number. As a result, EXAFS spectroscopy is quite sensitive to anharmonic effects and from it unique information about anharmonic interactions can be obtained.

We have used EXAFS to study the anharmonicity in CuBr at moderate temperatures. X-ray[5] and neutron diffraction[6] measurements on CuBr have shown that at room temperature the anharmonic motion of the Cu ions is significant. The mechanism responsible for this anharmonicity should be the same as that in CuCl, which exhibits anomalous behavior even at temperatures near absolute zero.[7-10] At high temperatures all of the cuprous halides become superionic conductors in which the Cu ions can diffuse through the lattice of halide ions.[11,12] It seems likely that the causes of the unusual high- and low-temperature behavior are related.

After reviewing anharmonic effects in the EXAFS spectrum and previous work on CuBr, we will discuss the experimental results and data analysis. The results will then be used to evaluate two models.

II. ANHARMONICITY AND EXAFS

For a polycrystalline material the K-edge EXAFS spectrum is described by[13]

$$\chi(k) = \sum_j \frac{S_0^2 N_j}{k} F_j(k)\,\mathrm{Im}\left(\frac{1}{r_j^2}e^{-2r_j/\lambda}e^{2ikr_j}\right)e^{i\delta_j(k)} , \qquad (2)$$

where k is the photoelectron wave number, S_0^2 is the square of the many-body overlap term, λ is the electron mean free path, and the sum is over the coordination shells of neighbors of the absorbing atom. $F(k)$ is the atomic backscattering amplitude and $\delta(k)$ is a net phase shift. If one expands the asymmetric terms in the brackets in a Taylor series about $R_j = \langle r_j \rangle$ and rewrites the thermal average in terms of cumulants, the result is[4]

$$\chi(k) = \sum_j \frac{S_0^2 N_j}{kR_j^2} F_j(k) \exp[-2(R_j/\lambda) - 2\sigma_j^2 k^2 + c_{ej}(k)]$$

$$\times \sin[2kR_j + \delta_j(k) + c_{oj}(k)] , \qquad (3)$$

where

$$c_{ej}(k) = \tfrac{2}{3}\sigma_j^{(4)} k^4 + \cdots , \qquad (4)$$

$$c_{oj}(k) = -\frac{4\sigma_j^2 k}{R_j}\left[1 + \frac{R_j}{\lambda}\right] - \tfrac{4}{3}\sigma_j^{(3)} k^3 + \cdots , \qquad (5)$$

and $\sigma_j^{(n)}$ denotes the nth cumulant.[14]

Although the first term on the right-hand side of Eq. (5) is important whenever σ^2 is large, the higher cumulant terms can be ignored as long as the quasiharmonic approximation gives an adequate description of the lattice-dynamical properties of the sample. However, when phonon-phonon interactions are important, the terms given in Eqs. (4) and (5) are required to give an accurate description of the EXAFS spectrum. Neglect of these terms can lead to significant errors in the interpretation of data.[15] For small anharmonicities, it may be sufficient to keep just the third and fourth cumulant terms. The fact that each term has a different k dependence and that even and odd cumulants are separated into the amplitude and phase, respectively, facilitates the determination of the cumulants from least-squares fits to the data. However, if more terms than this are important, the correlations between terms may make it impossible to get meaningful numbers for the cumulants.

III. PREVIOUS WORK ON CuBr AND RELATED COMPOUNDS

One can gain a better understanding of the unusual behavior of CuBr by comparing and contrasting it with the other noble-metal halides. According to Phillips,[16] cuprous and silver halides all have ionicities close to the critical value of 0.785 separating tetrahedrally- and octahedrally-coordinated binary crystals. At room temperature and atmospheric pressure, AgCl and AgBr are in the rock salt structure, while the cuprous halides all have the zinc-blende structure; AgI prefers the wurtzite structure but is metastable in the zinc-blende modification.[17] The tetrahedrally-coordinated crystals eventually transform to the rock salt structure under pressure. In the cuprous halides and AgI, unlike the other tetrahedral semiconductors, the metal d states have energies close to the anion p levels, and the valence bands involve strong p-d hybridization with substantial metal s character in the lowest conduction band.[18] The ionic conductivities of the noble-metal halides are quite significant at moderate temperatures,[11,19,20] and AgI (Ref. 21) and the cuprous halides[11] become superionic conductors at high temperatures. In the superionic phase of each material the metal atoms can diffuse through the lattice of halide ions.[12]

Several experimental techniques have been used to study the lattice dynamics of the cuprous halides. X-ray[5] and neutron[6] diffraction, inelastic neutron scattering,[22] and Raman[10,23,24] measurements all indicate that anharmonic

effects become important in CuBr for temperatures greater than 150 K. According to x-ray-diffraction measurements,[25] anharmonic behavior is not significant in CuI below 370 K, while room-temperature neutron-diffraction measurements[26] on CuCl reveal relatively strong anharmonicity. The most anomalous behavior is revealed by inelastic neutron scattering,[7,27] Raman,[8,10] and ir (Ref. 28) spectra for CuCl. Liquid-He temperature measurements reveal a splitting of the TO mode into two peaks for $q \sim 0$.

Several different models have been used to fit and explain the observations mentioned above. The x-ray- and neutron-diffraction data have been analyzed in terms of two models, a disorder model and a cubic anharmonic model.[5,6,25,26] In the former, the Cu ions are assumed to occupy off-center sites which are displaced from the normal equilibrium site along the [111] and the equivalent directions toward the faces of the coordination tetrahedron; there are four such sites per tetrahedron. The second model involves an anharmonic effective single-particle potential for each ion with terms higher than cubic neglected. For CuCl, from least-squares fits to integrated intensities of room-temperature neutron-diffraction Bragg peaks, together with analysis of the temperature dependence of the intensities of some of those lines, it was concluded that the cubic anharmonic model gave a better description of the data.[26] The cubic anharmonic model also gave a satisfactory fit to similar diffraction measurements made on CuBr, although in that case it was pointed out that quartic anharmonic terms would be needed to explain the damping of phonons in the [100] and [110] directions measured by inelastic neutron scattering.[6]

The TO phonon anomaly in CuCl has been explained[7,9,10,29-31] in terms of a model involving cubic anharmonic coupling between phonons. When the parameters are fitted to the data, the model gives a consistent explanation of the observations. Alternatively, Vardeny and Brafman[32] have invoked a modified disorder model to explain the anomalies observed in their Raman measurements. In their version, a Cu ion can sit at its ideal position as well as at the metastable off-center sites; a two-mode behavior of the optical phonons at $q \sim 0$ results. They also interpret a low-frequency peak observed in the Raman spectra of all three cuprous halides as a disorder-induced first-order TA mode.[33] The consequences of the model are extended to explain measurements on CuBr and CuI.

Although the differing models discussed have each had some success in providing a phenomenological explanation for the anharmonic behavior observed in the cuprous halides, none of them has shown explicitly how the required anharmonic potentials can be derived from the electronic and interatomic interactions from which such effects must arise. Some arguments have been given[33,34] which suggest that hybridization between Cu $3d$ and $4s$ and halogen p states may be quite sensitive to interatomic distance and might lead to attractive anharmonic forces between atom pairs. Related to this idea, anomalous broadening in ultraviolet photoemission measurements on CuBr (Ref. 35) and the silver halides[36] observed as a function of temperature has been explained in terms of fluctuations in p-d matrix elements between the metal and halo-

gen ions due to thermal fluctuations in the interatomic distance. These ideas are interesting, but one would like to be more quantitative. Calculations by Kleppmann and Weber[37] have shown that the quadrupolar deformability of Ag ions in the cubic silver halides arises from virtual d-s excitations at the Ag ions. The model has successfully explained some unusual features in the phonon-dispersion curves. One would like to find a similar sort of description for anharmonicity in the cuprous halides.

IV. EXPERIMENTAL PROCEDURE

CuBr in powder form (99.999% pure) was obtained from Apache Chemicals. After grinding, it was passed through a 400-mesh sieve and dusted uniformly onto Scotch Magic tape. A sample 10 tape layers thick was attached to a copper holder and mounted on the cold finger in a liquid-nitrogen cryostat. The sample had an x-ray thickness $\Delta\mu x$ of 1.6 at the Cu K edge and 1.1 at the Br K edge.

The absorption measurements were performed at the Stanford Synchrotron Radiation Laboratory (SSRL) on beam line VII-3 (a wiggler side station) with the storage ring (SPEAR) operating at 3.0 GeV and 60–80 mA and the wiggler magnet at 14 kG. A water-cooled Si 220 double-crystal monochromator determined the x-ray energy. At each absorption edge the monochromator was detuned so that the intensity of the monochromatized beam was 40% of maximum. The size of the beam seen by the detectors and sample was defined by a slit immediately following the monochromator. The incident and transmitted x-ray intensities were measured with ionization chambers filled with N_2 and Ar gas, respectively.

In analyzing EXAFS data, the zero of energy for the photoelectron is usually chosen to be associated with a particular feature at the edge. It is desirable to separate uncertainties in the energy-origin definition from inner-potential correction factors required in the data analysis to compensate for electronic changes. Since uncertainties of a few tenths of an electronvolt in energy origin can be a significant factor in determining the uncertainties in temperature or pressure-dependent distance changes, while monochromator and x-ray beam fluctuations can cause energy-scale shifts of more than a volt between scans, we decided to measure each sample edge position relative to a reference edge at room temperature. The Ni K edge of nickel foil and the Bi L_3 edge of bismuth foil were used as references for the Cu and Br edges, respectively. In the experiment, the reference material was mounted on a wheel, in front of the cryostat, so that it could be rotated into and out of the x-ray beam. A single scan through both reference and sample edges was made by scanning through the reference edge, rotating the reference out of the beam and continuing the scan through the sample edge. The positions of the features in the sample edge can then be measured relative to an inflection point or a peak in the reference edge.

A single "double-edge" reference scan and three full EXAFS scans were collected for both the Cu and Br edges at each temperature. The Cu-edge EXAFS were measured at 71 ± 3, 216 ± 3, and 295 ± 3 K, and the Br-edge scans were taken at 73 ± 3, 206 ± 7, and 295 ± 3 K.

V. DATA ANALYSIS

The first step in the data analysis is to extract $\mathcal{X}(k)$ from $\mu(E)x$. We start by determining the x-ray energy corresponding to the zero of photoelectron energy. From the double-edge reference scans we found that the first inflection point of each edge shifted less than 0.2 eV with temperature. The reproducibility of similar measurements on other samples suggests that the uncertainties in our relative edge position measurements are $\sim$0.2 eV, so we assumed that there were no significant edge shifts and set the energy origin to the position of the first inflection point for each scan. With this choice, $\mathcal{X}(k)$ is then obtained from $\mu(E)x$ by subtracting the background absorption (which is determined by fitting the data above the edge with a cubic spline) and normalizing to the edge step. The edge step is found by fitting straight lines to the data in the ranges from -300 to -100 eV and from 100 to 300 eV relative to the edge. The difference in the y values of these lines at the first inflection point is taken as the edge step. Measured in this way, we find that edge steps for all scans of each edge agree to within 1%. Typical room-temperature $\mathcal{X}(k)$ data (multiplied by k^3) are shown in Fig. 1.

In the next step, single-shell phase and amplitude data are obtained by Fourier filtering $\mathcal{X}(k)$. In the k to r transform, $\mathcal{X}(k)$ was weighted by k^3 and multiplied by a Gaussian centered on the square window and decaying to 0.1 at the edges. The transforms of the 72- and 210-K data are compared in Fig. 2. The first shell r-space peak between 1.4 and 2.9 Å was then transformed back to k space using a square window. The single-shell phase and amplitude data from the three scans of each edge at each
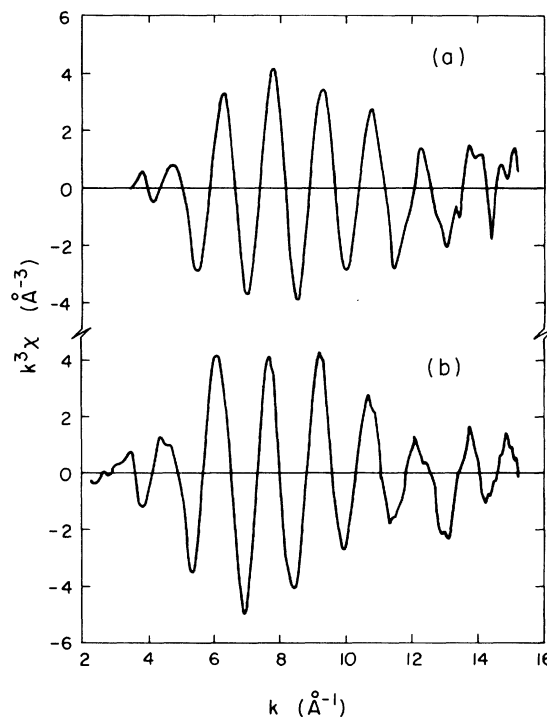

FIG. 1. Typical $k^3\mathcal{X}(k)$ data for CuBr at 295 K measured above the (a) Cu K edge, (b) Br K edge.
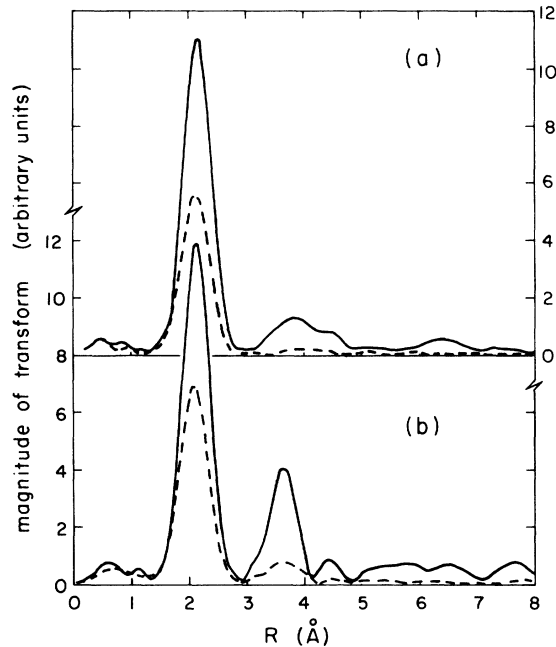
FIG. 2. Fourier transforms of the $k^3\chi(k)$ data weighted with a Gaussian. (a) Cu edge data, $T=71$ K (solid line), 216 K (dashed line); (b) Br edge data, $T=73$ K (solid line), 206 K (dashed line).

FIG. 3. Single-shell amplitude data plotted in the form $\ln[C(T_2)/C$ (72 K)]. (a) Cu edge data, $T_2=216$ K (circles), 295 K (triangles); (b) Br edge data, $T_2=206$ K (circles), 295 K (triangles). The dashed lines correspond to least-squares fits to the data with Eq. (6). Error bars used in the fitting are shown where they are larger than the symbol size.

temperature were averaged and the standard deviations were determined.

Once the single-shell phase and amplitude are isolated, the cumulants can be extracted using the ratio method.[2,38] If we multiply the amplitude $A(T)$ by the square of the distance $R(T)$ and call the product $C(T)$, then we expect to find

$$\ln[C(T_2)/C(T_1)] = -2\,\Delta\sigma^2 k^2 + \tfrac{2}{3}\sigma^{(4)}(T_2)k^4 , \qquad (6)$$

where $T_1=72$ K and it is assumed that all other terms in the amplitude do not change with temperature. We have also made the assumption that $\sigma^{(4)}(T_1)\approx 0$ for T_1, which seems reasonable in light of the low-temperature inelastic neutron scattering results.[26] In Fig. 3 our data is shown plotted in the form $\ln[C(T_2)/C(72$ K)] vs k^2. The thermal expansion measurements of Ref. 39 were used to get $R(T)$ (see Table II). We made least-squares fits, weighted by the error bars shown in the figure, with two different polynomials. The results are presented in Table I. The uncertainties shown correspond to the changes in the parameters when the fits are forced to go through y in-
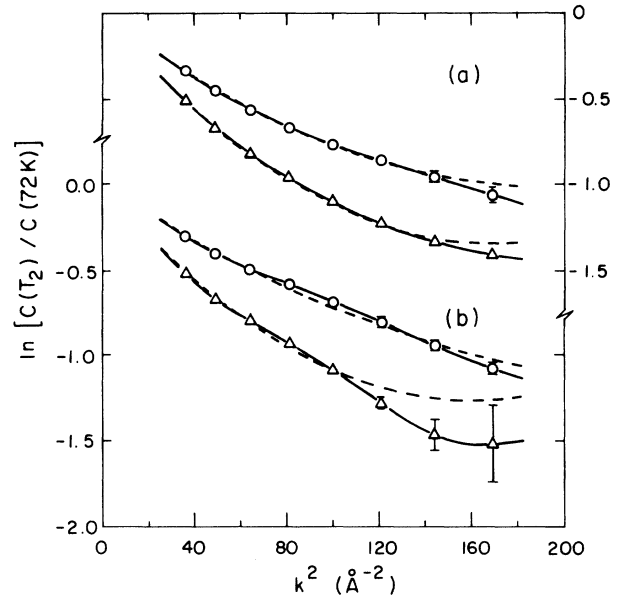
tercepts of ± 0.05. The polynomials corresponding to fit 2 are plotted with the data in Fig. 3. The results of fit 1 give a poor fit to the data and are included in Table I only to show what one gets if $\sigma^{(4)}$ is ignored. If the y intercept is included as a fitting parameter with $\Delta\sigma^2$, the values of $\Delta\sigma^2$ are found to be much smaller and the y intercepts are unreasonably low.

To obtain $\sigma^{(3)}$ we look at differences in the phase $\phi(T)$, for which we expect to find

$$\phi(T_2) - \phi(T_1) = 2k\left[\Delta R - \frac{2\,\Delta\sigma^2}{R}\left(1+\frac{R}{\lambda}\right)\right]$$

$$-\tfrac{4}{3}\sigma^{(3)}(T_2)k^3 . \qquad (7)$$

In writing down Eq. (7) we have assumed that the phase shifts cancel. The first term on the right-hand side of Eq. (7) can be written $2k\Delta R_{\text{eff}}$ where $\Delta R_{\text{eff}}=\Delta R_{\text{te}}+\Delta R_{\sigma^2}$, ΔR_{te} is the change in R due to thermal expansion, and

TABLE I. Results of fitting the data plotted in Fig. 3 with Eq. (6). In fit 1, $\sigma^{(4)}$ was constrained to be 0.

			Fit 1	Fit 2	
Edge	T_1 (K)	T_2 (K)	$\Delta\sigma^2$ (10^{-2} Å^2)	$\Delta\sigma^2$ (10^{-2} Å^2)	$\sigma^{(4)}$ (10^{-4} Å^4)
Br	73	206	0.36±0.03	0.44±0.07	0.24±0.11
Cu	71	216	0.40±0.03	0.52±0.07	0.40±0.13
Br	73	295	0.61±0.03	0.80±0.08	0.75±0.16
Cu	71	295	0.56±0.03	0.79±0.06	0.70±0.11

ΔR_{σ^2} represents the second term in the brackets. We removed this term from the phase differences using thermal expansion measurements[39] and the $\Delta\sigma^2$ values (fit 2) from Table I. A value of 8 Å was used for λ in ΔR_{σ^2}; this constant value is an approximation to the $\lambda(k)$ determined by Stern et al.[40] The ΔR values used are shown in Table II, where it can be seen that ΔR_{te} and ΔR_{σ^2} largely cancel each other.

We fitted the data with straight lines through the origin to illustrate the apparent anomalous contraction observed when $\sigma^{(3)}$ is ignored. To determine $\sigma^{(3)}$ we made least-squares fits including both ΔR and $\sigma^{(3)}$ as parameters, expecting the ΔR values to be near zero. We also made a third set of fits in which an inner potential term V_0 was used to adjust the k scales of the higher-temperature data sets so that $\Delta R = 0$. The adjusted k scale is given by

$$k' = \left[k^2 - \frac{2m}{\hbar^2} V_0 \right]^{1/2} . \tag{8}$$

Varying V_0 may correct for errors in the determination of the energy origin and can compensate for the effects of changes in electronic configurations on phase shifts.[41] The results of all three fits are presented in Table III. The data and the third set of fits are plotted in Fig. 4.

The values of $\Delta\sigma^2$ which we have obtained can be decomposed into a harmonic part $\Delta\sigma_H^2$ plus an anharmonic contribution $\Delta\sigma_A^2$. The harmonic part can be calculated from the phonon spectrum measured at low temperature. Calculations of $\Delta\sigma_H^2$ have been performed[42] for several tetrahedral semiconductors using published shell-model parameters which had been determined by least-squares fits to phonon-dispersion relations measured by inelastic neutron scattering. To give an idea of the accuracy of the models and measurements, the numbers obtained for Ge, GaAs, and ZnSe agree within 20% with the measurements of Stern et al.[40] For CuBr, a 14-parameter shell model fitted to neutron scattering measurements at 77 K by Hoshino et al.[22] (set II) was used. The results for the first and second shells are plotted in Fig. 5, and the numbers corresponding to the measured temperatures are presented in Table IV. After subtracting $\Delta\sigma_H^2$ from the $\Delta\sigma^2$ values (fit 2) in Table I, we obtain the results shown in Table V for σ^2, where we have averaged the numbers for the Br and Cu edges. We have also included in the table averaged results for $\sigma^{(3)}$ and $\sigma^{(4)}$.

The second-shell contributions to $\mathcal{X}(k)$ contain information about the Cu-Cu and Br-Br interatomic distance distributions. From Fig. 2 we see that the second-shell peaks are relatively small even at 72 K. The calculation of σ_H^2 shows that the mean-square relative displacements of
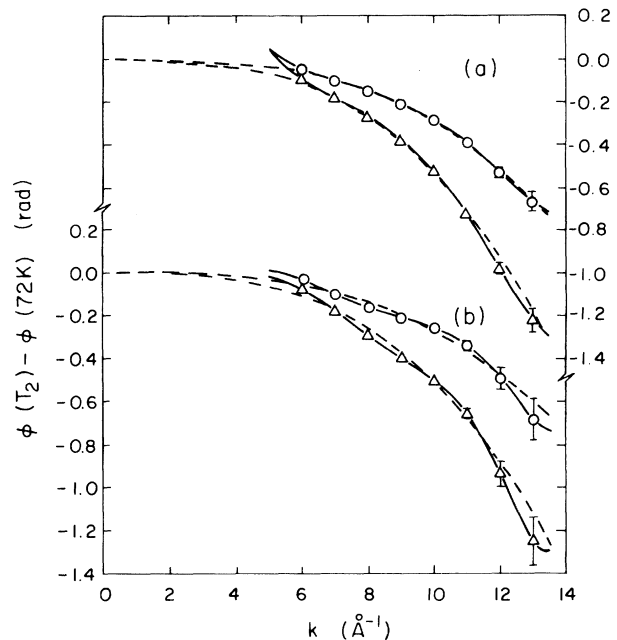

FIG. 4. Difference between single-shell phases at T_2 and 72 K. (a) Cu edge data, $T_2 = 216$ K (circles), 295 K (triangles); (b) Br edge data, $T_2 = 206$ K (circles), 295 K (triangles). The dashed lines correspond to least-squares fits to the data with Eq. (7). Error bars used in the fitting are shown where they are larger than the symbol size.

next-nearest neighbors are much larger than those of nearest neighbors and they increase rapidly with temperature. The strong thermal damping results in small amplitudes for the second-shell EXAFS and at higher temperatures makes it difficult to analyze these shells quantitatively; such analysis is nevertheless worth an attempt.

The second-shell contributions were Fourier filtered the same way as the first, except that an r-space window extending from 3.15 to 4.15 Å was used. At the Br edge, using the 73-K data as reference, we obtain $\Delta\sigma^2$ values of

TABLE II. Real and effective distances entering the EXAFS single-shell phase difference (Eq. 7). The notation is explained in the text.

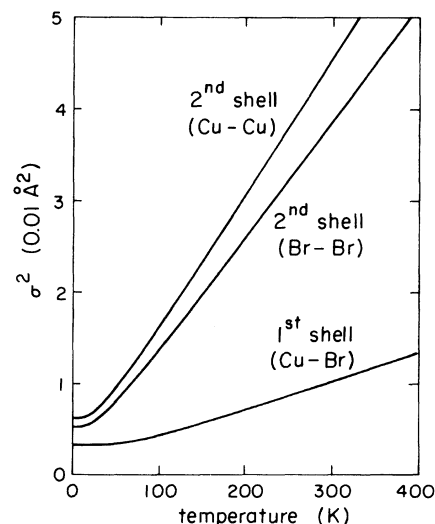| T_1 (K)	T_2 (K)	ΔR_{te} (Å)	ΔR_{σ^2} (Å)	ΔR_{eff} (Å)
72	210	0.003	−0.005	−0.002
72	295	0.006	−0.008	−0.002

FIG. 5. Results of the shell-model calculation of the mean-square relative displacements in CuBr.

TABLE III. Results of least-squares fits to the phase difference data (Fig. 4).

Edge	T_1 (K)	T_2 (K)	Fit 1 ΔR (Å)	Fit 2 ΔR (Å)	$\sigma^{(3)}(2)$ $(10^{-3}$ Å$^3)$	Fit 3 $V_0(2)$ (eV)	$\sigma^{(3)}(2)$ $(10^{-3}$ Å$^3)$
Br	73	206	−0.008	0.004	0.25	−0.5	0.21
Cu	71	216	−0.009	0.001	0.23	−0.1	0.23
Br	73	295	−0.024	−0.003	0.35	0.4	0.38
Cu	71	295	−0.020	−0.004	0.36	0.5	0.40

0.0145±0.0025 and 0.027±0.005 Å^2 at 206 and 295 K, respectively. The Cu edge second-shell data was in the noise at 215 K so that no reliable determination of $\Delta\sigma^2$ could be made. Comparison of the measured $\Delta\sigma^2$ values for the Br edge with the calculated ones in Table IV indicates quite good agreement. The observed and calculated results for the Cu edge also seem to be in agreement in that the mean-square relative displacement for second-neighbor Cu atom pairs is significantly larger than that for Br atom pairs. This fact suggests that the anharmonic effects may be related to the large motion of the Cu atoms.

VI. DISCUSSION

From Figs. 3 and 4 we see that the nearest-neighbor distance distribution measured by EXAFS is well described by an expansion in which only the first few cumulant moments are retained. It is also clear that $\sigma^{(3)}$ and $\sigma^{(4)}$ are quite significant even at 210 K and that substantial errors in the determination of distance and σ^2 would be made if anharmonic corrections were left out of the analysis. Because of the simple way in which the terms in Eqs. (6) and (7) can be separated according to their different k dependences, it is apparent that the determination of the higher moments is most easily performed in k space using the ratio method.

For an ideal harmonic crystalline lattice, the cumulants beyond σ^2 are effectively zero, and the value of σ^2 at any temperature can be calculated from a temperature-independent projected density of phonon states. In a quasiharmonic model, the force constants change with temperature due to thermal expansion, which leads to an anharmonic correction to σ_H^2 for the harmonic lattice. Above the Debye temperature, one can use an argument analogous to the one given by Willis and Pryor[43] for the mean-square displacement $\langle u^2 \rangle$ to show that

$$\Delta\sigma^2 = \Delta\sigma_H^2 \left[1 + 2\gamma_G \frac{\Delta V}{V} \right] \quad (9)$$

where γ_G is an appropriate Grüneisen parameter and $\Delta V/V$ is the relative volume change due to thermal expansion. For CuBr, we can estimate γ_G from the measured[44] Grüneisen parameters for the optical modes to be about 2.5, and using the thermal expansion results[39] we find that the correction factor between 72 and 295 K is 1.039. Hence, the contribution to $\Delta\sigma_A^2$ due to thermal expansion is roughly 0.02×10^{-2} Å^2. The rest of $\Delta\sigma_A^2$ must be due to temperature-dependent static disorder or intrinsic anharmonicity.

We would like to fit the terms σ_A^2, $\sigma^{(3)}$, and $\sigma^{(4)}$ to a model. We will first consider the disorder model, in which we assume that the four off-center sites are located a distance Δ away from the central site, and that a Cu atom spends a fraction f of its time at off-center sites and $(1-f)$ at the ideal site. (The distribution can be smoothed by convolution with a Gaussian; the cumulants of the two distributions are additive.[4]) Δ and f are assumed to be temperature dependent. The nth cumulant of the distribution is proportional to Δ^n and appears in $\chi(k)$ multiplied by k^n. It follows that we can ignore higher-order moments only when $k\Delta \ll 1$. The first few cumulants are, to lowest order in Δ/R,

$$\sigma^2 = \tfrac{1}{3} f\Delta^2 , \quad (10a)$$

$$\sigma^{(3)} = \tfrac{2}{9} f\Delta^3 , \quad (10b)$$

$$\sigma^{(4)} = \left[\frac{7-9f}{27} \right] f\Delta^4 . \quad (10c)$$

Fitting f and Δ to the room-temperature cumulant values in Table V, we find $f = 0.08$, $\Delta = 0.26$ Å; the corresponding cumulant values are $\sigma^2 = 0.18 \times 10^{-2}$ Å^2, $\sigma^{(3)} = 0.31 \times 10^{-3}$ Å^3, and $\sigma^{(4)} = 0.85 \times 10^{-4}$ Å^4. We obtain a reasonable fit to the three values with two parameters. However, $1/\Delta = 4$ Å^{-1} and hence many higher cumulants should be important in the experimental-data range. This means that if the disorder model is appropri-

TABLE IV. Results of shell-model calculation of mean-square relative displacements for CuBr.

Edge	T_1 (K)	T_2 (K)	$\Delta\sigma^2$ First shell $(10^{-2}$ Å$^2)$	$\Delta\sigma^2$ Second shell $(10^{-2}$ Å$^2)$
Br	73	206	0.356	1.65
Cu	71	216	0.384	2.08
Br	73	295	0.629	2.77
Cu	71	295	0.629	3.26

TABLE V. Averaged results for σ_A^2, $\sigma^{(3)}$ and $\sigma^{(4)}$.

T (K)	σ_A^2 $(10^{-2}$ Å$^2)$	$\sigma^{(3)}$ $(10^{-3}$ Å$^3)$	$\sigma^{(4)}$ $(10^{-4}$ Å$^4)$
210	0.11±0.08	0.23±0.04	0.32±0.12
295	0.16±0.12	0.37±0.05	0.72±0.12

ate we should observe beats in the single-shell EXAFS spectrum due to interference between the contributions to $\chi(k)$ from Cu atoms at the three different radial distances from a Br atom. We can include all cumulants by writing

$$\langle e^{2ik(r-R)}\rangle = Ae^{i\phi} = (1-f) + \frac{f}{4}(e^{2ik\Delta} + 3e^{-2ik\Delta'}) , \qquad (11)$$

where $\Delta' \approx \frac{1}{3}\Delta$. Substituting the f and Δ values determined above into Eq. (11), we obtain the phase and amplitude (solid line) shown in Fig. 6. There is a minimum in the amplitude near 8 Å^{-1} and neither the phase nor amplitude gives a good description of the data at high k. In order to get a good fit to the phase, we must shift the minimum in the phase out of the observed k range by decreasing Δ. To obtain reasonable cumulants, f must increase to compensate for Δ. Setting f equal to its maximum value of 1, we find that $\Delta=0.105$ Å gives a reasonable fit to the measured phase (short-dashed line in Fig. 6). However, the resulting σ^2 value for the model calculated over the experimental data range, 0.47×10^{-2} Å^2, is much too large (compared to $\sigma_A^2=0.14\times10^{-2}$ Å^{-2}), while $\sigma^{(4)}$ comes out too small (0.49 compared to 0.72×10^4 Å^4). If Δ is increased by much the phase fit becomes poor while a good fit to the amplitude is difficult to obtain for any pair
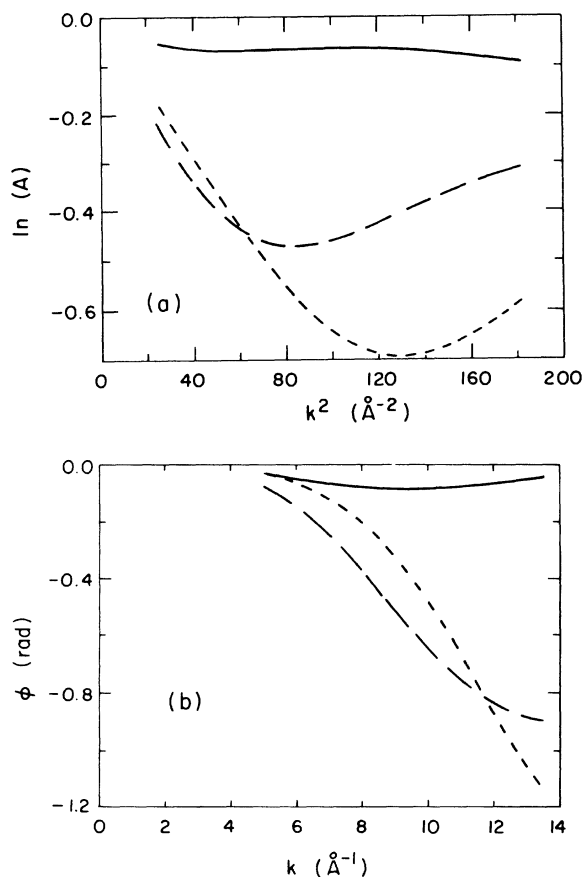

FIG. 6. Calculations of amplitude and phase contributions due to the disorder model using Eq. (11) with $f=0.08$, $\Delta=0.26$ A (solid line); $f=1.0$, $\Delta=0.105$ A (short-dashed line); $f=0.60$, $\Delta=0.16$ A (long-dashed line).

of f and Δ values. The results for a pair of intermediate values ($f=0.60$, $\Delta=0.16$ Å) are indicated by the long-dashed line in Fig. 6. Hence we conclude that off-center potential minima do not exist in CuBr at 300 K and lower temperatures. It could be argued that such minima do exist but that the Cu ions spend much of their time moving between minima; however, from our data it appears that the ions would spend so much time in motion that the off-center sites picture has little meaning.

Having rejected the disorder model, we turn to anharmonic models. The proper approach to applying anharmonicity would be to write the cumulant moments in terms of normal coordinates and then fit the values of the Fourier-transformed third- and fourth-order potentials to our data. There are several problems with this approach, however. For one thing, the multiple Brillouin-zone integrations are quite complicated to perform, in general. More importantly, though, it is not trivial to find a meaningful approximation for the cubic and quartic potentials which properly describes the data, allows only Cu-ion anharmonic motion, and involves a small number of free parameters. Instead, we will consider an effective anharmonic single-particle potential. Such a model does not give an accurate description of the situation because it ignores correlated motion, but it may provide some qualitative understanding of our results.

The anharmonic single-particle potential with the appropriate symmetry can be written

$$V(\vec{u}) = V_0(\vec{u}) + V_A(\vec{u}) , \qquad (12)$$

where

$$V_0(\vec{u}) = \frac{1}{2}\alpha u^2 \qquad (13)$$

and

$$V_A(\vec{u}) = \beta xyz + \gamma u^4 + \delta(x^4+y^4+z^3 - \frac{3}{5}u^4) , \qquad (14)$$

and where $\vec{u}$ is the displacement of a Cu ion from its equilibrium position. Such a model, neglecting the quartic terms, has been applied to neutron-diffraction data[6] and EXAFS measurements[45] on CuBr at high temperature. The cumulants for such a potential are

$$\sigma^2 = \sigma_0^2 + \sigma_0^4 \left[-20\frac{\gamma}{\alpha} + \left[\frac{\beta}{\alpha}\right]^2 \right] , \qquad (15a)$$

$$\sigma^{(3)} = -\frac{2\sqrt{3}}{3}\sigma_0^4\frac{\beta}{\alpha} , \qquad (15b)$$

$$\sigma^{(4)} = \sigma_0^6 \left[-24\frac{\gamma}{\alpha} + \frac{32\delta}{5\alpha} + 4\left[\frac{\beta}{\alpha}\right]^2 \right] , \qquad (15c)$$

where $\sigma_0^2 = \langle u^2\rangle_0 = kT/\alpha$. If we assume that the Br ions see a harmonic potential and we ignore contributions from correlation terms, we can fit the Cu ion anharmonic potential terms to the room-temperature cumulants in Table V (with σ_A^2 adjusted for thermal expansion). Using $\langle u_{Cu}^2\rangle_0 = 0.0441$ Å^2,[6] we find $\beta/\alpha = -0.16$ Å^{-1}, $\gamma/\alpha = -0.035$ Å^{-2} and $\delta/\alpha = -0.100$ Å^{-2} Our value for β/α is quite small compared to the ratio of ~1.2 obtained by Harada et al.[6] However, if we set $\gamma/\alpha=0$ in Eq. (15a) then fitting σ_A^2 alone requires $|\beta/\alpha|=0.85$ Å^{-1}. The

comparison suggests that the quartic potential is quite important and that the value of β obtained by Harada *et al.* is much too large because it must compensate for neglect of the fourth-order terms.

The effective single-particle potential model gives us a prediction of the temperature dependence of each cumulant moment. From Eqs. (15) it can be seen that σ_A^2 and $\sigma^{(3)}$ are proportional to T^2 and that $\sigma^{(4)}$ is proportional to T^3. If we scale our average room-temperature values for the moments according to these relations, we get values of $\sigma_A^2 = 0.07 \times 10^{-2}$ Å^2, $\sigma^{(3)} = 0.19 \times 10^{-3}$ Å^3, and $\sigma^{(4)} = 0.26 \times 10^{-4}$ Å^4 at 210 K, in good agreement with our measurements. Scaling the values of 72 K indicates that our assumption that the higher cumulants are negligible at that temperature is a good one. The model appears to give a reasonable description of the temperature dependence of the data.

VII. SUMMARY

We have measured EXAFS spectra at the Cu and Br edges in CuBr at 72, 210, and 295 K. From analysis of Fourier-filtered first-shell data using the ratio method, we have obtained values for the cumulants σ_A^2, $\sigma^{(3)}$, and $\sigma^{(4)}$ which are nonzero due to anharmonicity. The data should be sensitive to the presence of Cu atoms sitting at off-center sites, but we see no evidence for statically disordered Cu ions. Instead we find, ignoring the contributions from correlation terms, that the experimental results are consistent with an effective anharmonic single-particle potential for the Cu ions. The analysis clearly shows that the quartic potential terms are just as important as the cubic for describing anharmonic behavior at moderate temperatures in CuBr.

[1]E. A. Stern, Contemp. Phys. **19**, 289 (1978); P. A. Lee, P. H. Citrin, P. Eisenberger, and B. M. Kincaid, Rev. Mod. Phys. **53**, 769 (1981).

[2]E. A. Stern, D. E. Sayers, and F. W. Lytle, Phys. Rev. B **11**, 4836 (1975).

[3]G. Beni and P. M. Platzman, Phys. Rev. B **14**, 1514 (1976).

[4]J. J. Rehr (unpublished).

[5]S. Hoshino, J. Phys. Soc. Jpn. **7**, 560 (1952).

[6]J. Harada, H. Suzuki, and S. Hoshino, J. Phys. Soc. Jpn. **41**, 1707 (1976).

[7]B. Hennion, B. Prevot, M. Krauzman, R. M. Pick, and B. Dorner, J. Phys. C **12**, 1609 (1979).

[8]J. E. Potts, R. C. Hanson, C. T. Walker, and C. Schwab, Phys. Rev. **9**, 2711 (1974).

[9]M. Krauzman, R. M. Pick. H. Poulet, G. Hamel, and B. Prevot, Phys. Rev. Lett. **33**, 528 (1974).

[10]T. Fukumoto, S. Nakashima, K. Tabuchi, and A. Mitsuishi, Phys. Status Solidi B **73**, 341 (1976).

[11]J. B. Wagner and C. Wagner, J. Chem. Phys. **26**, 1597 (1957).

[12]J. B. Boyce and T. M. Hayes, *EXAFS Spectroscopy: Techniques and Applications*, edited by P. K. Teo and D. C. Joy (Plenum, New York, 1981), p. 103.

[13]E. A. Stern, Phys. Rev. B **10**, 3027 (1974); P. A. Lee and J. B. Pendry, *ibid.* **11**, 2795 (1975); C. A. Ashley and S. Doniach, *ibid.* **11**, 1279 (1975); E. A. Stern, B. A. Bunker, and S. M. Heald, *ibid.* **21**, 5521 (1980).

[14]The cumulants $\sigma^{(n)}$ are defined by the equation

$$\langle e^{2ikr} \rangle = \exp \left[\sum_{n=1}^{\infty} [(2ik)^n/n!] \sigma^{(n)} \right] .$$

Expressions for the cumulants in terms of the moments about the mean μ_n are given in Ref. 4. We have chosen to write $\sigma^2 = \sigma^{(2)}$. In statistics books, the notation κ_n is often used for the nth cumulant.

[15]P. Eisenberger and G. S. Brown, Solid State Commun. **29**, 481 (1979).

[16]J. C. Phillips, Rev. Mod. Phys. **42**, 317 (1970).

[17]C. W. F. T. Pistorius, Prog. Solid State Chem. **11**, 1 (1976).

[18]A. Goldman, Phys. Status Solidi B **81**, 9 (1977).

[19]R. J. Friauf, J. Phys. (Paris) **38**, 1077 (1977).

[20]H. Hoshino and M. Shimoji, J. Phys. Chem. Solids **35**, 321 (1974).

[21]P. C. Allen and D. Lazarus, Phys. Rev. B **17**, 1913 (1978).

[22]S. Hoshino, Y. Fujii, J. Harada, and J. D. Axe, J. Phys. Soc. Jpn. **41**, 965 (1976).

[23]J. E. Potts, R. C. Hanson, C. T. Walker, and C. Schwab, Solid State Commun. **13**, 389 (1973).

[24]E. M. Turner, I. P. Kaminow, and C. Schwab, Phys. Rev. B **9**, 2524 (1974).

[25]S. Miyake, S. Hoshino, and T. Takenaka, J. Phys. Soc. Jpn. **7**, 19 (1952).

[26]M. Sakata, S. Hoshino, and J. Harada, Acta Crystallog. A **30**, 655 (1974).

[27]B. Prevot, B. Hennion, and B. Dorner, J. Phys. C **10**, 3999 (1977).

[28]M. Ikezawa, J. Phys. Soc. Jpn. **35**, 309 (1973).

[29]M. L. Shand, H. D. Hochheimer, M. Krauzman, J. E. Potts, R. C. Hanson, and C. T. Walker, Phys. Rev. B **14**, 4637 (1976).

[30]R. C. Hanson and M. L. Shand, *Proceedings of the 6th AIRAPT International High Pressure Conference*, edited by K. D. Timmerhaus and M. S. Barber (Plenum, New York, 1979), p. 453.

[31]J. Ruvalds and A. Zawadowski, Phys. Rev. B **2**, 1172 (1970).

[32]Z. Vardeny and O. Brafman, Phys. Rev. B **19**, 3276 (1979).

[33]Z. Vardeny and O. Brafman, Phys. Rev. B **19**, 3290 (1979).

[34]G. Gilat, Phys. Lett. **81A**, 68 (1981).

[35]S. F. Lin, W. E. Spicer, and R. S. Bauer, Phys. Rev. B **14**, 4551 (1976).

[36]R. S. Bauer and W. E. Spicer, Phys. Rev. B **14**, 4539 (1976).

[37]W. G. Kleppmann and W. Weber, Phys. Rev. B **20**, 1669

(1979).

[38]G. Bunker, Nucl. Instrum. Methods 207, 437 (1983).

[39]H. P. Schaake, AFCRL Report No. 69-0538 (unpublished), quoted by J. N. Plendl and L. C. Mansur, in Appl. Opt. 11, 1194 (1972).

[40]E. A. Stern, B. A. Bunker and S. M. Heald, Phys. Rev. B 21, 5521 (1980).

[41]B. K. Teo and P. A. Lee, J. Am. Chem. Soc. 101, 2815 (1979).

[42]J. M. Tranquada and J. J. Rehr (unpublished).

[43]B. T. M. Willis and A. W. Pryor, *Thermal Vibrations in Crystallography* (Cambridge Unversity Press, London, 1975).

[44]H. D. Hochheimer, M. L. Shand, J. E. Potts, R. C. Hanson, and C. T. Walker, Phys. Rev. B 14, 4630 (1976).

[45]J. B. Boyce, T. M. Hayes, and J. C. Mikkelson, Jr. Solid State Commun. 35, 237 (1980).